# Quasistatic Shape Adjustment of a 15-Meter-Diameter Space Antenna

W. Keith Belvin*
*NASA Langley Research Center, Hampton, Virginia*
Harold H. Edighoffer†
*Edighoffer, Inc., Newport News, Virginia*
and
Catherine L. Herstrom‡
*NASA Langley Research Center, Hampton Virginia*

**A 15-m-diam hoop-column antenna has been analyzed and tested to study shape adjustment of the reflector surface. The hoop-column antenna concept employs pretensioned cables and mesh to produce a paraboloidal reflector surface. Fabrication errors can distort the surface of mesh-type reflectors significantly, which ultimately degrades the electromagnetic performance of the antenna. To improve antenna performance, a shape-adjustment procedure to reduce surface distortions was developed. The shape-adjustment algorithm consisted of finite-element and least-squares error analyses. Experimental results verified the analysis procedure. Application of the procedure resulted in reduction of the average surface error by 36% in two iterations. Quasistatic shape adjustment has the potential for on-orbit compensation for a variety of surface-shape distortions.**

## Nomenclature

$e$ = surface coordinate error vector
$F$ = focal length of paraboloid
$I$ = mass moment of inertia
$S$ = matrix of mesh/cable influence coefficients
$\Delta u$ = cable length change vector
$V_x, V_y$ = coordinates of desired paraboloid vertex
$W$ = diagonal weighting matrix
$x,y,z$ = three components of rectangular surface coordinates
$z^m$ = measured vector of $z$-direction surface coordinates
$z^i$ = ideal vector of $z$-direction surface coordinates for perfect paraboloid

## Introduction

A NUMBER of large space antennas have been proposed for communications, remote sensing, and other science applications as described, for example, in Refs. 1-3. Major design considerations for space antennas are the mass and deployment of the structural system. Both the mass and packaged volume of the antenna system are limited by the size and mass capabilities of launch and transport vehicles. Hence, lightweight deployable antenna concepts have received considerable attention in the literature. In addition to mass and deployment considerations, the electromagnetic (EM) performance of the antenna, which is directly related to the surface accuracy, must be considered. Reference 4 shows that a distorted reflector surface degrades the EM performance. The surface-accuracy effects become more pronounced as the EM operating frequency increases. Thus, the deployed surface accuracy of space antennas is of paramount importance.

Unlike Earth-based antennas that use rigid reflector surfaces, space-antenna designs frequently employ mesh surfaces to minimize mass and to facilitate deployment. Mesh surfaces are not easily shaped into curved surfaces because of negligible bending stiffness in the mesh. Nevertheless, mesh surfaces can be deformed with cables into shapes that approximate paraboloidal surfaces. The cables are attached at one end to the mesh and at the opposite end to a stiff part of the antenna structure.

Antennas designed with mesh/cable reflector surfaces possess three major sources of surface distortions. First, the number of cables used is finite, which results in only an approximation to the desired paraboloidal surface. Fortunately, the surface error resulting from the use of a finite number of control cables can be estimated, and the number of cables can be selected based on a specified error tolerance. Second, dimensional fabrication errors in structural components can result in significant surface distortions. Third, thermal or vibration excitation of the antenna can produce local surface distortions as well as global defocusing of the antenna. Surface distortions resulting from fabrication errors cannot be predicted a priori. Hence, measurement of the surface must be made subsequent to the fabrication, and surface adjustments made if necessary. One method for surface adjustment is to use control (adjustable) cables to reshape the surface. Similarly, thermal and vibration excitation often produce distortions that are difficult to predict. Thus, measurement of the surface distortions and adjustment of control cables may be required.

One large space-antenna concept that has been fabricated and tested is the hoop-column antenna.[5,6] A 15-m-diam antenna was fabricated for electromagnetic and structural testing

Presented as Paper 87-0869 at the AIAA/ASME/ASCE/AHS 28th Structures, Structural Dynamics, and Materials Conference, Monterey, CA, April 6-8, 1987; received Sept. 8, 1987; revision received Sept. 19, 1988. 

*Aerospace Engineer, Spacecraft Dynamics Branch, Structural Dynamics Division. Member AIAA.
†President. Member AIAA.
‡Computer Technologist, Structural Concepts Branch, Structural Mechanics Division.

and for verification of the deployment concept. Even though the antenna was constructed using state-of-the-art fabrication techniques, surface distortions were significant. Hence, an analysis was developed to reduce the surface error by changing the surface control-cable lengths. Three iterations of quasi-static shape adjustment were experimentally performed. This paper documents the analysis and experimental results of surface shape adjustment on the 15-m hoop-column antenna. Finite-element and least-squares error analyses are described followed by a discussion of experimental results. In addition, a brief discussion of the antenna structural dynamics is presented for consideration in future real-time shape control.

## Antenna Description

The 15-m hoop-column antenna is shown in Fig. 1. The reflector surface consists of four paraboloidal apertures, each of which occupies a 90-deg segment or one quadrant of the antenna. The mesh surface is divided into 24 gores, which are shaped by control cables. The surface-error budget (0.069 in.) and mesh size were chosen to permit electromagnetic testing from 2.225–11.6 GHz. The antenna size was chosen to permit both electromagnetic and structural tests to be performed in existing ground test facilities. An extensive description of the antenna exists in the literature[1,5-7]; hence, only a brief description is presented herein.

The antenna was designed to be stowed in the shuttle cargo bay and deployed on-orbit. Deployment occurs from a cylindrical package, 0.9 m in diameter and 2.7 m in length. The deployed antenna size is 15 m in diameter and 9.5 m in height. Figure 2 shows the antenna deployment sequence. The packaged antenna is mounted on a tripod support for ground test deployment. The column telescopes simultaneously from both top and bottom. After the column is deployed, the hoop is deployed by eight motors that are mounted in eight of the 24 hoop joints. (Counterbalances on the hoop are used to compensate for gravity effects during ground deployment.) The final deployment step is the actuation of a preload segment at the bottom of the column. This segment extends outward to pretension all of the cables and mesh, thus providing a stable-deployed configuration as shown in Fig. 1. Figure 3 shows a schematic of the major antenna components.

Lightweight materials have been used to fabricate the antenna. The hoop and column tubes are made of graphite-epoxy construction. However, the joints between members and the cable stowage spools at the top and bottom of the column are made of aluminum. All cables are made from unidirectional graphite or quartz filaments. The surface mesh is made of gold-plated molybdenum wire. Table 1 lists the weights of the antenna subassemblies. The total mass of the antenna, including instrumentation, is 410.0 kg (904.0 lb) with the center of gravity located at 1.78 m above the hoop. The rotational inertias of the antenna are $I_x = I_y = 11523$ kg-m$^2$ (101910 lb-s$^2$-in.) and $I_z = 7966$ kg-m$^2$ (70445 lb-s$^2$-in.).

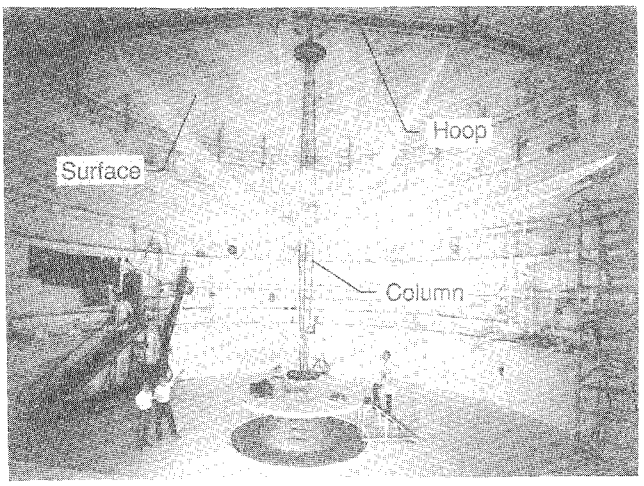


Fig. 1 15-m-diam hoop-column antenna.

## Structural Modeling

The antenna was designed with 96 surface control cables that could be adjusted in length to minimize the surface error. To compute the control-cable length changes needed to minimize the surface error, an analytical model was required to determine the influence of each control-cable adjustment on the surface shape. Thus, a finite-element structural model was developed and used to compute a matrix of influence coefficients, which related the 888 surface-target displacements to adjustments of control-cable lengths. Figure 4 shows the target locations of one aperture that were used in the analysis. The "effective surface area," shown in Fig. 4, is described in the Results and Discussion section.

The Engineering Analysis Language (EAL) finite-element program[8] was used to model the structural behavior of the antenna. Figure 5 shows the analytical model without the surface mesh and control cables. The hoop, column, and tripod were modeled with beam elements, whereas the cables were modeled with rod elements. Effects of axial member loads on the antenna stiffness were modeled by including the differential stiffness. Member preloads were based on fabrication drawings and were not updated using measured data. Since the antenna was tested in ground facilities, gravity loading was included in all analyses. The model shown in Fig. 5 was verified by dynamic tests before installation of the surface mesh.[1]

Modeling of the surface required 4664 rod elements and 2880 two-dimensional triangular membrane elements. Since the antenna has four apertures and 24 gores, the smallest substructure that can be used with reflective and rotational symmetry to model the antenna surface is the three-gore model shown in Fig. 6a. Reflective symmetry of the three-gore model produces one complete aperture (quadrant) as shown in Fig.

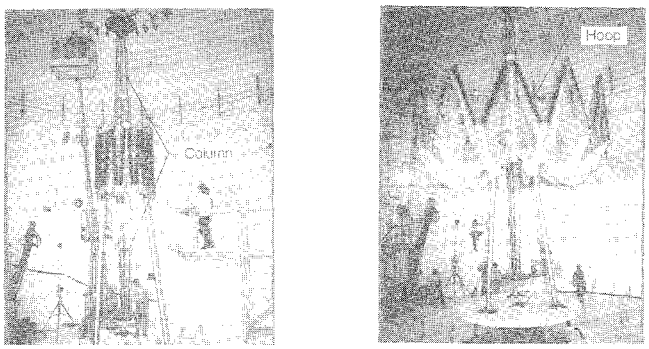


Column deployed Hoop partially deployed

Fig. 2 Antenna deployment sequence.

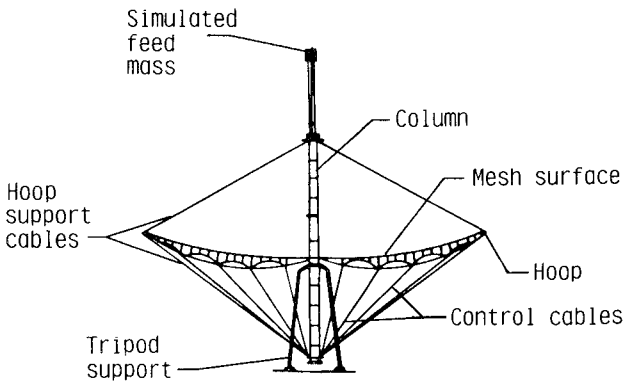


Fig. 3 Major components of antenna.

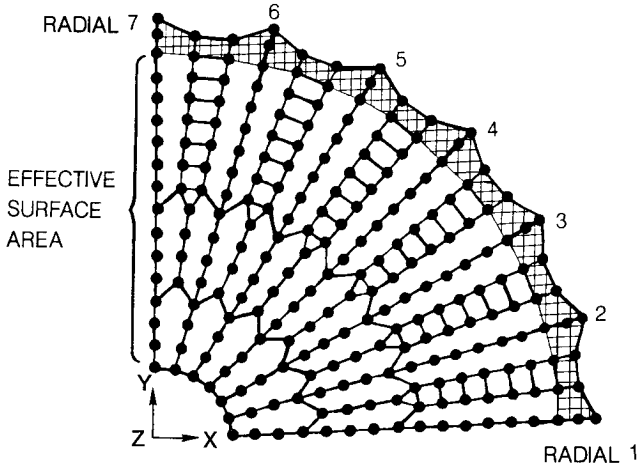


Fig. 4 Surface-target locations.

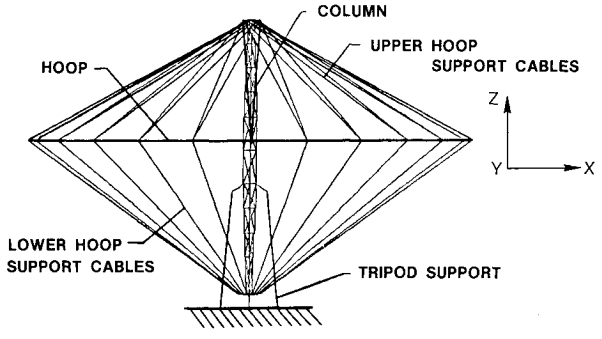


Fig. 5 Finite-element model without surface.

Table 1 Subassembly Weights

| Elements | Mass (weight) |
|---|---|
| Hoop (graphite) | 136.6 kg (301.1 lb) |
| Column (graphite) | 141.6 kg (312.2 lb) |
| Surface mesh (gold plated molybdenum wire) | 9.1 kg (20.1 lb) |
| Cables (graphite and quartz) | 3.2 kg (7.1 lb) |
| Feed mast (steel) | 11.5 kg (25.4 lb) |
| Simulated feed weight | 108.0 kg (238.0 lb) |
| | Total 410.0 kg (903.9 lb) |

6b. Repeated application of rotational symmetry was used to produce the model of the entire surface as shown in Fig. 6c (for clarity, only membrane elements are shown in Fig. 6c). The surface model was merged with the model of the hoop and column (Fig. 5) to permit structural modeling of the complete antenna.

Nodal coordinates of the surface were chosen to achieve the desired paraboloidal shape. Member preloads were designed to maintain the paraboloidal shape in the presence of gravity. Static analysis using the finite-element model showed the equilibrated surface shape differed from the design shape by a root-mean-square (rms) average of 0.007 in. The baseline surface error (0.007 in. rms) could be reduced by changing the member preloads. However, the baseline model was not further refined, since the antenna surface-error budget was 0.069 in. rms.

## Mesh/Cable Influence Coefficients

Static analysis of the model was performed to determine the effect of cable adjustments on the surface shape. The control

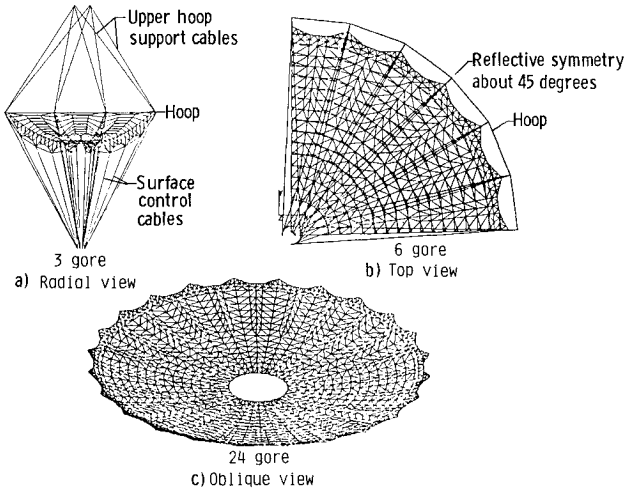


Fig. 6 Finite-element model of surface.

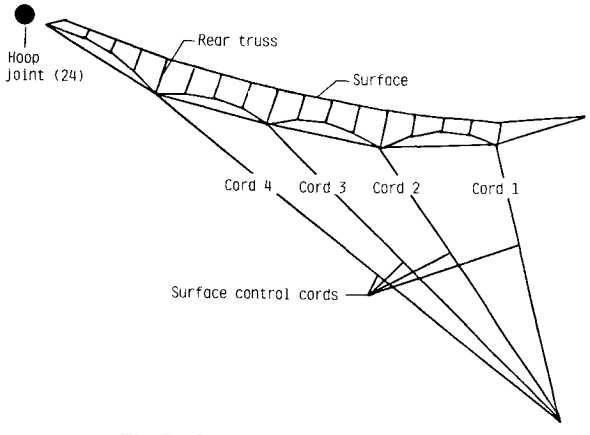


Fig. 7 Surface control-cable geometry.

cables, shown in Fig. 7, were individually shortened in the analytical model using an artificial thermal strain, and the resulting change in surface-target locations relative to the baseline model were computed. The 888 surface-target displacements, resulting from a unit control-cable adjustment, formed a column in the matrix of influence coefficients [$S$]. Individual unit cable adjustments were repeated in the analysis until the matrix of influence coefficients for one quadrant (888 targets × 24 cables) was assembled. Rotational symmetry was used to expand the matrix for the complete antenna surface (888 × 96). Typical control-cable effects on the displacements of the surface targets in the vertical direction are shown in Fig. 8. The surface-target displacements of Fig. 8 are the result of lengthening the cables by

Radial 4-Cord 1 = 1.00 in.
Radial 10-Cord 2 = 0.75 in.
Radial 16-Cord 3 = 0.50 in.
Radial 22-Cord 4 = 0.25 in.

The effect of cable-length adjustments on the surface shape is generally local. The sensitivity of surface-target locations to cable-length changes is higher in outboard cables than the inboard cable. Although inboard cables are more nearly vertical, outboard cables have higher sensitivity, because the change in cable tension (lateral stiffness) becomes the dominant parameter effecting the surface-target displacements.

## Surface-Adjustment Analysis

Minimization of the antenna surface error can be performed using the cable influence coefficients [S] computed in the previous section. Examination of the influence coefficients showed that control-cable adjustments produce predominantly vertical ($z$) motion with very small $x$ and $y$ target motion. Thus, the analysis was simplified by neglecting $x$ and $y$ target motion and accounting for $z$ motion only. The design paraboloidal shape is given by

$$z_j = [(x_j - V_x)^2 + (y_j - V_y)^2]/F \quad (1)$$

where $x_j$, $y_j$, and $z_j$ are the perfect paraboloid coordinates of the $j$th target, $F$ is the focal length = 366.85 in., and $V_x, V_y$ is the vertex offset,

| | | |
|---|---|---|
| Quadrant 1: | $V_x = 10.39$ in. | $V_y = 10.39$ in. |
| Quadrant 2: | $V_x = -10.39$ in. | $V_y = 10.39$ in. |
| Quadrant 3: | $V_x = -10.39$ in. | $V_y = -10.39$ in. |
| Quadrant 4: | $V_x = 10.39$ in. | $V_y = -10.39$ in. |

The measured $x$- and $y$-coordinate values ($x^m$, $y^m$) of the surface targets were substituted into Eq. (1) to obtain the ideal $z$ coordinates $z^i$. Thus, the vertical surface-shape error ($e$) is

$$e_j = (z_j^i - z_j^m) \quad (2)$$

The effect of the control cables on the surface is given by

$$[S]\ \{\Delta u\} = \{\Delta z\} \quad (3)$$

where $\{\Delta u\}$ is a vector of 96 control-cable length changes and $\{\Delta z\}$ is a vector of vertical displacements of the 888 surface targets. Thus, given a vertical surface error to be corrected, $\{e\}$, a set of compensating control-cable adjustments $\{\Delta u\}$ may be computed using least-squares error analysis of the following form

$$[S]^T\ [W]\ [S]\ \{\Delta u\} = [S]^T\ [W]\ \{e\} \quad (4)$$

where $[W]$ is a diagonal weighting matrix. Equation (4) represents a set of 96 simultaneous equations that may be solved to obtain the best set of control-cable adjustments $\{\Delta u\}$ to minimize a given surface error $\{e\}$. In practice, Eq. (4) should be solved in the form

$$[W]\ [S]\ \{\Delta u\} = [W]\ \{e\} \quad (5)$$

as an overdetermined system of equations to help avoid numerical conditioning problems. For example, the form given by Eq. (5) can be solved directly in a least-squares sense by using a singular-value decomposition procedure.

## Results and Discussion

Before electromagnetic testing at a large near-field facility,[9] convergent close-range photogrammetric measurements were made from eight locations, 7 m above the hoop, to determine the location of 888 surface targets. The measured surface data consisted of three rectangular coordinates for each target, accurate to 0.007 in. in each direction. For each aperture, the targets located in the "effective surface area" (see Fig. 4) were used to compute best-fit paraboloidal parameters, namely, the rms error, vertex location, and focal point. This subset of targets was chosen because they give a better indication of EM performance than does the full target complement. Hence, the surface-accuracy results given herein are from a best-fit paraboloid to the targets in the "effective surface area." Figure 9 shows a contour plot of the measured surface error in the vertical direction. The contour plots for each of the four quadrants were curve-fitted individually; thus, some discontinuities exist at quadrant boundaries.

Analysis of the measured data indicated that significant deviation from the desired surface accuracy existed. The average four-quadrant rms surface error was 0.121 in., which exceeded the design error tolerance of 0.069 in. by 75%. The surface-adjustment analysis described previously was used to compute

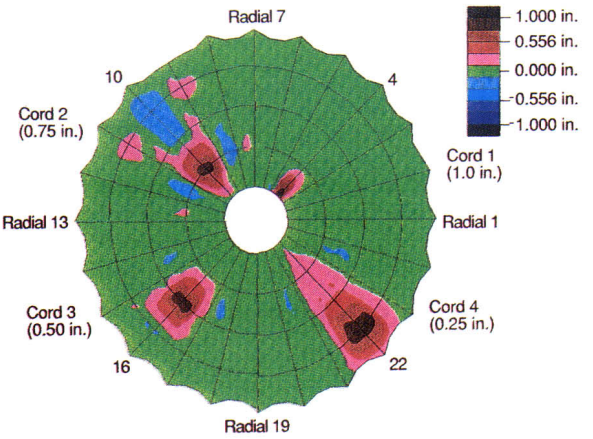


**Fig. 8 Typical surface displacements resulting from cable-length adjustment.**

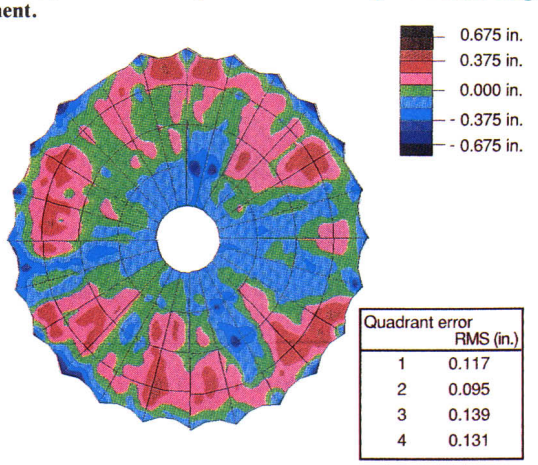


**Fig. 9 Surface error prior to cable adjustment.**

**Table 2 96 cable-length changes computed for first surface adjustment**

| Radial | Cord 1 | Cord 2 | Cord 3 | Cord 4 |
|---|---|---|---|---|
| 1 | 0.149 | 0.151 | 0.092 | −0.035 |
| 2 | 0.142 | 0.080 | 0.022 | 0.034 |
| 3 | 0.160 | 0.089 | 0.026 | −0.083 |
| 4 | 0.199 | −0.029 | −0.086 | −0.004 |
| 5 | 0.196 | 0.069 | −0.040 | −0.041 |
| 6 | 0.215 | 0.310 | 0.073 | −0.003 |
| 7 | 0.191 | 0.150 | 0.013 | −0.060 |
| 8 | 0.270 | 0.047 | 0.009 | −0.011 |
| 9 | 0.212 | 0.075 | −0.030 | −0.041 |
| 10 | 0.162 | 0.055 | −0.014 | 0.017 |
| 11 | 0.161 | 0.058 | 0.020 | −0.058 |
| 12 | 0.145 | 0.039 | −0.007 | −0.054 |
| 13 | 0.128 | 0.149 | 0.027 | −0.036 |
| 14 | 0.178 | 0.048 | 0.042 | 0.059 |
| 15 | 0.159 | 0.069 | −0.042 | −0.065 |
| 16 | −0.001 | 0.031 | −0.069 | −0.005 |
| 17 | 0.216 | −0.006 | 0.096 | −0.013 |
| 18 | 0.142 | 0.005 | −0.076 | −0.068 |
| 19 | 0.192 | 0.034 | 0.030 | −0.035 |
| 20 | 0.175 | 0.157 | 0.012 | −0.056 |
| 21 | 0.228 | 0.129 | 0.192 | 0.014 |
| 22 | 0.143 | 0.043 | −0.025 | −0.096 |
| 23 | 0.242 | 0.047 | 0.175 | −0.058 |
| 24 | 0.255 | 0.040 | 0.033 | 0.031 |

cable-length changes to minimize the measured surface error. Experimental implementation of the cable adjustments was performed by relaxing a set screw on the cable fittings and using vernier calipers to measure the cable motion as required. Each cable was adjusted sequentially and a full 96 cable adjustment took a team of three people about 7 h to perform.

The following sections describe results from three experiments using the surface-adjustment procedure. The first two iterations used unity weighting ($[W]$ was equal to the identity matrix), whereas the third iteration used non-unity weighting.

**Case 1: 96 Cable Adjustment**

The measured target-coordinate data of Fig. 9 was input to the surface-adjustment analysis, and the cable-length changes listed in Table 2 were computed. These cable adjustments produce the surface displacement shown in Fig. 10. The predicted shape after adjustment is obtained by adding the surface displacement of Fig. 10 to Fig. 9, which yields the surface-error contour of Fig. 11. The predicted rms error after adjustment has an average value of 0.082 in. for the effective surface area.

The cable adjustments of Table 2 exceeding 0.011 in. were implemented, and the antenna surface shape was remeasured. (Cable adjustments below 0.011 in. were not deemed practical because of the manual adjustment procedure used in the experiment.) The measured error after adjustment is shown in Fig. 12. The contour plots are not identical for the predicted surface error (Fig. 11) and measured surface error (Fig. 12). However, the rms error levels show good agreement, except for aperture D (quadrant 4). During the experimental implementation of the cable adjustments, one cable in aperture D was inadvertently not adjusted (radial 21–cord 3). Thus, a second iteration of the cable-adjustment procedure was performed.

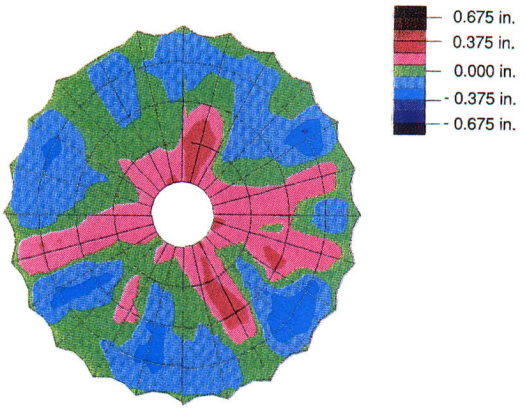


**Fig. 10 Surface displacements predicted for first cable adjustment (96 cables).**

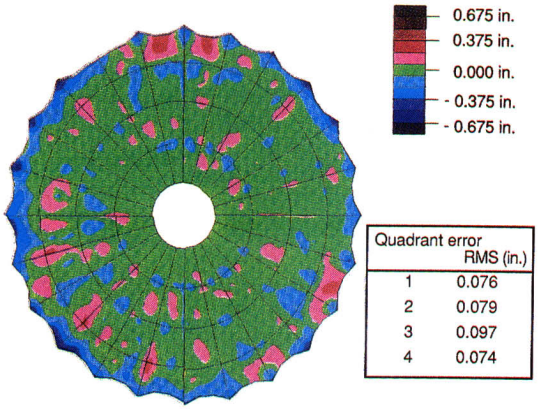


**Fig. 11 Predicted surface error after first cable adjustment (96 cables).**

**Case 2: 10 Cable Adjustment**

The second iteration to improve the antenna surface accuracy produced a set of cable adjustments as shown in Table 3. In addition to the cable that was skipped, other cable adjustments were of sufficient magnitude to warrant readjustment. This indicated that modeling errors were present, since linear analysis should converge in one iteration. Although the $[S]$ matrix could be identified experimentally, the high cost of measuring the antenna surface with photogrammetry techniques precluded this option. Thus, each iteration of the surface-adjustment procedure used the same influence coefficients even though some degree of modeling error was known to be present.

The control cables whose adjustments exceeded 0.040 in. were chosen to be readjusted. The shape-control algorithm was modified to permit a subset of the 96 cables to be adjusted. Ten cable adjustments were recomputed as listed in Table 4. These 10 cable adjustments were predicted to produce the error contour as shown in Fig. 13. After the 10 cables were experimentally adjusted, the surface shape was measured and found to yield the error contour of Fig. 14. A comparison of Figs. 14 and 13 show the measured and predicted rms errors to be in good agreement.

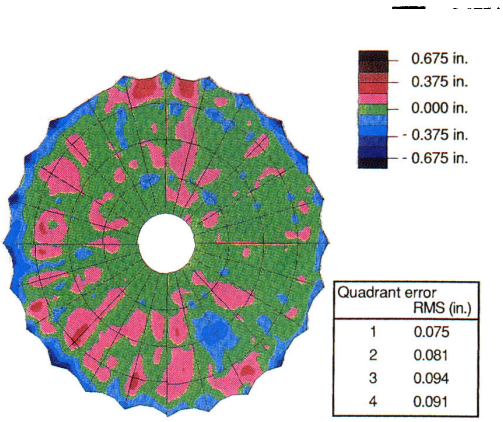


**Fig. 12 Measured surface error after first cable adjustment (85 t (85 cables).**

**Table 3 96 cable-length changes computed for second surface adjustment**

| Radial | Cord 1 | Cord 2 | Cord 3 | Cord 4 |
|---|---|---|---|---|
| 1 | − 0.026 | − 0.014 | − 0.004 | − 0.015 |
| 2 | − 0.024 | − 0.014 | 0.010 | 0.003 |
| 3 | − 0.055 | − 0.005 | − 0.003 | − 0.014 |
| 4 | − 0.098 | 0.030 | 0.004 | 0.002 |
| 5 | − 0.017 | − 0.068 | 0.005 | 0.008 |
| 6 | − 0.015 | − 0.029 | − 0.029 | − 0.004 |
| 7 | − 0.002 | 0.080 | − 0.017 | − 0.013 |
| 8 | − 0.019 | − 0.053 | 0.004 | − 0.010 |
| 9 | − 0.021 | − 0.024 | − 0.008 | 0.003 |
| 10 | − 0.020 | − 0.002 | − 0.011 | − 0.005 |
| 11 | − 0.005 | − 0.022 | − 0.016 | − 0.022 |
| 12 | − 0.009 | − 0.065 | − 0.021 | − 0.001 |
| 13 | − 0.002 | − 0.037 | − 0.018 | − 0.008 |
| 14 | − 0.017 | − 0.019 | − 0.012 | 0.014 |
| 15 | − 0.006 | − 0.028 | − 0.006 | − 0.026 |
| 16 | − 0.034 | 0.010 | − 0.038 | − 0.006 |
| 17 | − 0.002 | 0.010 | − 0.042 | − 0.018 |
| 18 | − 0.022 | − 0.039 | − 0.019 | − 0.009 |
| 19 | − 0.045 | − 0.029 | − 0.031 | − 0.022 |
| 20 | − 0.020 | − 0.020 | − 0.011 | − 0.018 |
| 21 | − 0.019 | − 0.011 | 0.222 | − 0.020 |
| 22 | − 0.038 | − 0.080 | − 0.032 | − 0.009 |
| 23 | − 0.027 | − 0.011 | − 0.034 | 0.009 |
| 24 | 0.010 | 0.026 | − 0.021 | 0.004 |

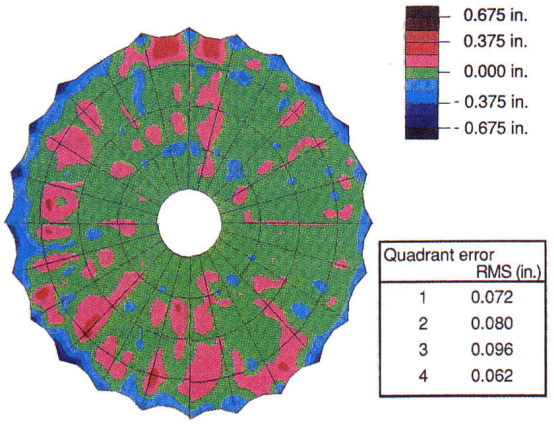


Fig. 13 Predicted surface error after second cable adjustment (10 cables).

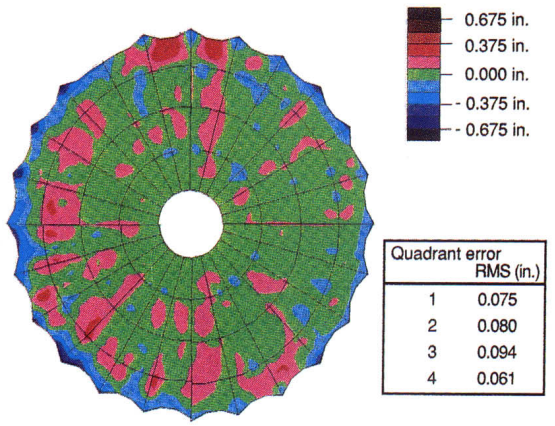


Fig. 14 Measured surface errors after second cable adjustment (10

The measured data of Fig. 14 was used to compute another iteration of 96 cable adjustments as listed in Table 5. These new cable adjustments were small, and the analysis predicted that they would have little effect on the rms error. Thus, the cable adjustments of Table 5 were not performed.

#### Case 3: Weighted Surface-Error Cable Adjustment

The feed-horn design of the antenna produced a pattern of electromagnetic energy on the reflector as shown in Fig. 15. The electromagnetic performance of the antenna is directly related to the surface accuracy in this region. Thus, a final adjustment of the surface control cables was computed and performed, using the Bessel function magnitude of Fig. 15 to form the weighting matrix $[W]$ in Eq. (4). Table 6 lists the 96 cable adjustments computed using the weighted surface error. From this table, the cable adjustments exceeding 0.020 in. were chosen to be adjusted. Table 7 lists the 33 cable adjustments that were experimentally performed. Although the predicted (Fig. 16) and measured surface error showed only a 2% decrease in average rms error from the previous iteration, the antenna performance improved after the third cable adjustment by reducing the electromagnetic-energy side lobes by 15 dB.[6] These results indicate that in addition to overall rms surface errors, local surface distortions can also degrade antenna performance. Thus, weighting of the surface error by the local electromagnetic energy distribution does improve antenna performance.

## Antenna Dynamics

The shape-adjustment results presented herein assumed that the antenna could be modeled with static analysis. This assumption is permissible if the rate of control-cable changes is

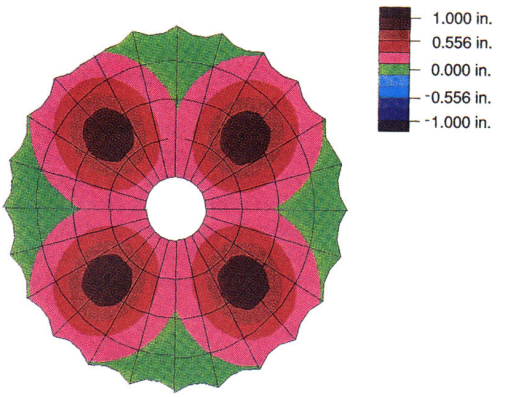


Fig. 15 Electromagnetic energy distribution used to weigh the surface error.

Table 4 10 cable-length changes implemented in second surface adjustment

| Radial | Cord 1 | Cord 2 | Cord 3 | Cord 4 |
|---|---|---|---|---|
| 1 | 0.000 | 0.000 | 0.000 | 0.000 |
| 2 | 0.000 | 0.000 | 0.000 | 0.000 |
| 3 | −0.059 | 0.000 | 0.000 | 0.000 |
| 4 | −0.084 | 0.000 | 0.000 | 0.000 |
| 5 | 0.000 | −0.058 | 0.000 | 0.000 |
| 6 | 0.000 | 0.000 | 0.000 | 0.000 |
| 7 | 0.000 | −0.092 | 0.000 | 0.000 |
| 8 | 0.000 | 0.042 | 0.000 | 0.000 |
| 9 | 0.000 | 0.000 | 0.000 | 0.000 |
| 10 | 0.000 | 0.000 | 0.000 | 0.000 |
| 11 | 0.000 | 0.000 | 0.000 | 0.000 |
| 12 | 0.000 | −0.090 | 0.000 | 0.000 |
| 13 | 0.000 | 0.000 | 0.000 | 0.000 |
| 14 | 0.000 | 0.000 | 0.000 | 0.000 |
| 15 | 0.000 | 0.000 | 0.000 | 0.000 |
| 16 | 0.000 | 0.000 | 0.000 | 0.000 |
| 17 | 0.000 | 0.000 | −0.069 | 0.000 |
| 18 | 0.000 | 0.000 | 0.000 | 0.000 |
| 19 | −0.072 | 0.000 | 0.000 | 0.000 |
| 20 | 0.000 | 0.000 | 0.000 | 0.000 |
| 21 | 0.000 | 0.000 | 0.185 | 0.000 |
| 22 | 0.000 | −0.099 | 0.000 | 0.000 |
| 23 | 0.000 | 0.000 | 0.000 | 0.000 |
| 24 | 0.000 | 0.000 | 0.000 | 0.000 |

Table 5 96 cable-length changes computed after 10 cable adjustment

| Radial | Cord 1 | Cord 2 | Cord 3 | Cord 4 |
|---|---|---|---|---|
| 1 | −0.033 | −0.016 | −0.009 | −0.015 |
| 2 | −0.020 | −0.013 | 0.012 | 0.004 |
| 3 | −0.003 | −0.008 | −0.008 | −0.016 |
| 4 | −0.014 | 0.032 | 0.003 | 0.002 |
| 5 | −0.002 | −0.043 | 0.011 | 0.014 |
| 6 | −0.019 | −0.017 | −0.028 | −0.008 |
| 7 | 0.026 | −0.040 | −0.016 | −0.011 |
| 8 | −0.029 | 0.015 | 0.005 | −0.017 |
| 9 | −0.009 | −0.032 | −0.004 | 0.007 |
| 10 | −0.017 | 0.002 | −0.013 | −0.009 |
| 11 | −0.001 | −0.016 | −0.012 | −0.018 |
| 12 | −0.003 | 0.014 | −0.022 | −0.005 |
| 13 | −0.001 | −0.035 | −0.027 | −0.017 |
| 14 | −0.015 | −0.018 | −0.019 | 0.008 |
| 15 | 0.000 | −0.028 | −0.007 | −0.024 |
| 16 | −0.031 | 0.015 | −0.037 | −0.003 |
| 17 | 0.005 | 0.002 | 0.020 | −0.017 |
| 18 | −0.015 | −0.029 | −0.014 | 0.002 |
| 19 | −0.008 | −0.024 | −0.028 | 0.022 |
| 20 | −0.012 | −0.041 | −0.011 | −0.017 |
| 21 | −0.031 | 0.000 | 0.043 | −0.019 |
| 22 | −0.024 | −0.012 | −0.032 | −0.004 |
| 23 | −0.041 | −0.006 | −0.032 | 0.010 |
| 24 | 0.009 | 0.026 | −0.016 | 0.017 |

very small relative to the structural vibration frequencies. When active shape adjustment is desired, the dynamics of the antenna must be considered. This section describes typical vibration characteristics of the antenna.

The antenna was vibration tested using low-level excitation to determine modal vibration parameters.[10] In addition, the finite-element model described previously was used to predict the frequencies and mode shapes. The analytical model predicted 70 vibration modes dominated by surface-mesh displacements from 4.1–6.2 Hz. Figure 17 shows typical mode shapes predicted by the analysis. Experimentally, these modes were found to be highly damped and coupled. Although some amplification of the frequency-response measurements occurs in this range, the experimental data were not successfully reduced into a set of recognizable mode shapes. The complexity of the antenna surface leads to uncertainties in the analytical model. For example, the differential stiffness may be in error because of member preloads being affected by fabrication tolerances. In addition, ground vibration testing is difficult because of the large size and high damping of the mesh. Thus, a simple model of the mesh was tested to verify the membrane analysis, and to quantitatively estimate the mesh damping.

A 1.2 m square-mesh model was pretensioned to 3.01 N/m and vibration tested in both air and vacuum conditions. Modal damping for the first mode was approximately 9 and 7% for the square-mesh model when tested with and without ambient air, respectively.[10] This level of damping, coupled with high

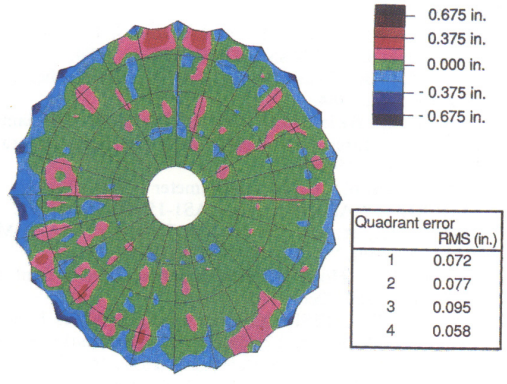


Fig. 16 Predicted surface error after third cable adjustment (weighted error, 33 cables).

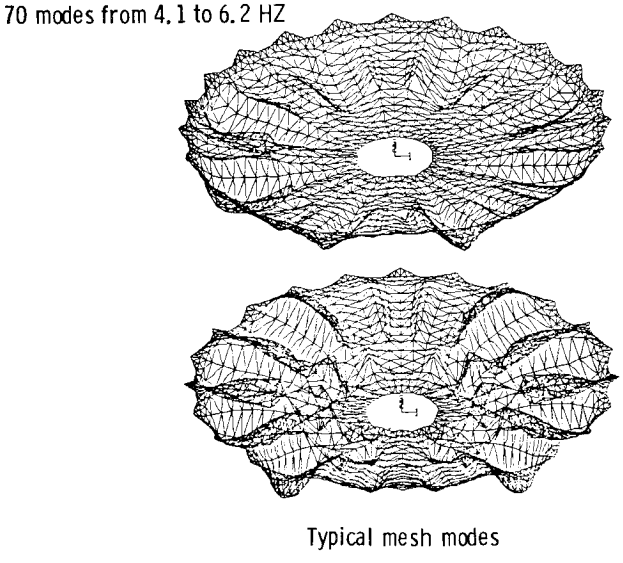


Fig. 17 Analytical mode shapes dominated by surface-mesh motion.

Table 6 96 cable-length changes computed for weighted surface adjustment

| Radial | Cord 1 | Cord 2 | Cord 3 | Cord 4 |
|---|---|---|---|---|
| 1 | −0.043 | −0.011 | −0.006 | −0.017 |
| 2 | −0.026 | −0.015 | 0.014 | 0.007 |
| 3 | −0.046 | −0.001 | −0.007 | −0.019 |
| 4 | 0.020 | 0.025 | 0.012 | 0.000 |
| 5 | −0.021 | −0.040 | 0.002 | 0.014 |
| 6 | −0.043 | −0.026 | −0.036 | 0.006 |
| 7 | 0.024 | −0.039 | −0.037 | −0.012 |
| 8 | −0.031 | 0.003 | −0.022 | 0.004 |
| 9 | −0.009 | −0.034 | −0.009 | 0.005 |
| 10 | −0.001 | 0.001 | 0.004 | −0.016 |
| 11 | −0.013 | −0.015 | −0.004 | −0.026 |
| 12 | −0.005 | 0.016 | −0.008 | −0.010 |
| 13 | −0.003 | −0.022 | 0.034 | −0.042 |
| 14 | −0.012 | −0.014 | −0.029 | 0.000 |
| 15 | −0.010 | −0.025 | −0.005 | −0.012 |
| 16 | −0.021 | 0.009 | −0.028 | −0.019 |
| 17 | −0.002 | 0.012 | 0.031 | −0.016 |
| 18 | −0.016 | −0.039 | −0.038 | 0.004 |
| 19 | −0.008 | −0.015 | −0.019 | −0.024 |
| 20 | −0.022 | −0.050 | −0.001 | −0.023 |
| 21 | −0.048 | 0.006 | 0.034 | −0.012 |
| 22 | −0.021 | −0.021 | −0.034 | −0.006 |
| 23 | −0.043 | −0.006 | −0.042 | 0.018 |
| 24 | 0.017 | 0.027 | −0.021 | 0.014 |

Table 7 33 cable-length changes implemented in weighted surface adjustment

| Radial | Cord 1 | Cord 2 | Cord 3 | Cord 4 |
|---|---|---|---|---|
| 1 | −0.059 | 0.000 | 0.000 | 0.000 |
| 2 | −0.040 | 0.000 | 0.000 | 0.000 |
| 3 | −0.046 | 0.000 | 0.000 | 0.000 |
| 4 | 0.000 | 0.024 | 0.000 | 0.000 |
| 5 | −0.049 | 0.000 | 0.000 | 0.000 |
| 6 | −0.040 | −0.022 | −0.031 | 0.000 |
| 7 | 0.022 | −0.051 | −0.052 | 0.000 |
| 8 | −0.026 | 0.000 | 0.000 | 0.000 |
| 9 | 0.000 | −0.047 | 0.000 | 0.000 |
| 10 | 0.000 | 0.000 | 0.000 | 0.000 |
| 11 | 0.000 | 0.000 | 0.000 | −0.033 |
| 12 | 0.000 | 0.000 | 0.000 | 0.000 |
| 13 | 0.000 | −0.030 | 0.037 | −0.045 |
| 14 | 0.000 | 0.000 | −0.034 | 0.000 |
| 15 | 0.000 | −0.039 | 0.000 | 0.000 |
| 16 | 0.000 | 0.000 | −0.054 | 0.000 |
| 17 | 0.000 | 0.000 | 0.000 | 0.000 |
| 18 | 0.000 | −0.040 | −0.033 | 0.000 |
| 19 | 0.000 | 0.000 | 0.000 | −0.032 |
| 20 | −0.019 | −0.054 | 0.000 | −0.026 |
| 21 | −0.046 | 0.000 | 0.023 | 0.000 |
| 22 | −0.021 | −0.025 | −0.047 | 0.000 |
| 23 | −0.037 | 0.000 | 0.000 | 0.000 |
| 24 | 0.000 | 0.032 | 0.000 | 0.000 |

Table 8 Antenna modes with cable suspension and feed mast

| | Analysis (reduced model) | Test | | |
|---|---|---|---|---|
| Mode | F, Hz | F, Hz | C/CR, % | Mode shape |
| 1 (2) | 0.132 | 0.138 | 3.1 | First pendulum |
| 2 (2) | 0.283 | 0.284 | 1.2 | Second pendulum |
| 3 (2) | 1.47 | 1.47 | 1.3 | Hoop rocking/ column and feed mast bending |
| 4 | 2.20 | 2.19 | 1.1 | Column/hoop torsion |
| 5 (2) | 4.37 | 4.09 | 1.9 | Second column and feed mast bending |
| 6 | 5.40 | 5.42 | 0.94 | Feed mast torsion |

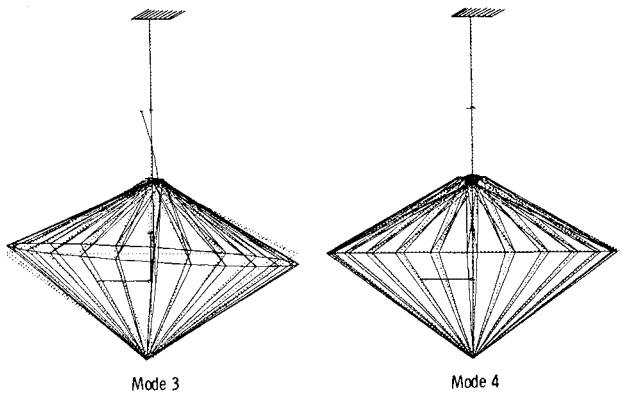


**Fig. 18 Analytical mode shapes dominated by hoop and column motion (surface not shown).**

modal density of the mesh modes, will make verification of the antenna dynamic model difficult. The square-mesh model frequencies were predicted reasonably well; hence, membrane theory is believed to be sufficient for estimating the mesh frequencies and mode shapes.

In addition to mesh vibration modes, there exist vibration modes that involve column and hoop motion, which can defocus the antenna by moving the focal point of the paraboloid relative to the feed location. Figure 18 shows two vibration modes of this type. The antenna (with surface) was suspended by a pendulum cable for these tests to simulate more closely the free-free boundary conditions of space. Table 8 shows that the analysis predicts the modes dominated by hoop and column motion quite well. (Modes with a 2 in parentheses indicates repeated frequencies caused by symmetry.) The modes dominated by hoop and column motion must also be considered in an active shape control system because of their low frequency and effect on EM performance.

## Summary

The 15-m hoop-column antenna permits surface-shape adjustment by changing the control-cable lengths. A method for quasistatic surface adjustment of the antenna, based on finite-element and least-squares error analyses, has been developed. Analysis and test results using quasistatic surface adjustment have been presented.

The antenna surface-shape behavior is predicted well with linear finite-element analysis. Predicted and measured surface rms error levels agree within 4%. The average surface error for all four apertures was reduced by 38% in two iterations of control-cable adjustments. The surface rms error of the best aperture was reduced from 0.131 to 0.061 in. after two iterations.

Surface adjustment was based on the availability of 888 surface-target measurements and the least-squares solution of 96 simultaneous equations. Studies have not yet been performed for reduced-order modeling. However, the localized behavior of the mesh/cable interaction should lead to simplifying assumptions to reduce the problem size. Automation of the shape-control procedure using cable actuators for cable adjustment and near real-time sensors of surface-target measurements is underway. Modifications of the quasistatic surface-adjustment analysis will be required for active control due to antenna dynamics. Nevertheless, the quasistatic tests have shown shape control is feasible, and the present analysis could be used to compensate for a variety of surface distortions.

Antenna surface-shape control permits compensation for fabrication, thermal, and other surface distortions, and appears to be quite practical for large space antennas. The as-built surface accuracy of the 15-m hoop-column antenna indicates that fabrication errors can be significant. Thus, future large space-antenna designs should consider hardware and software requirements to enable on-orbit surface-shape control.

## References

[1]Campbell, T. G., Butler, D. H., Belvin, W. K., and Allen B., "Development of the 15-m Hoop-Column Antenna Concept," NASA CP-2368, Dec. 1984.

[2]Freeland, R. E., Garcia, N. F., and Iwamoto, H., "Wrap-Rib Technology Development," NASA CP-2368, Dec. 1984.

[3]Coyner, J. V., "Box Truss Development and Its Applications," NASA CP-2368, Dec. 1984.

[4]Grantham, W. L., Bailey, M. C., Belvin, W. K., and Williams, J. P., "Controls-Structures-Electromagnetics-Interaction Program," NASA CP-2447, Nov. 1986.

[5]Harris Corporation, "15-Meter-Diameter Hoop-Column Antenna," Final Rept., NASA Contract NAS1-15763, June 1986.

[6]Schroeder, L. C., et. al., "Near-Field Testing of the 15-Meter Hoop-Column Antenna," NASA TM-4073, 1988.

[7]Sullivan, M. R., "Hoop-Column Antenna Development Program," NASA CP-2269, Dec. 1982.

[8]Whetstone, W. D., "EISI-EAL Engineering Analysis Language Reference Manual," Vols. 1 and 2, Engineering Information Systems, Inc., San Jose, CA, EISI-EAL System Level 2091, July 1983.

[9]Martin Marietta Corporation, "Near-Field Testing of 15 Meter Model of the Hoop-Column Antenna," NASA CR-178059, March 1986.

[10]Belvin, W. K. and Edighoffer, H. E., "15-Meter Hoop Column Antenna Dynamics: Test and Analysis," NASA CP-2447, Nov. 1986.

**Color reproduction courtesy of NASA Langley Research Center**